Water Mist Spray Characterization and Its Proper Application for Numerical Simulations

BENJAMIN DITCH and HONG-ZENG YU
FM Global Technologies
1151 Boston-Providence Turnpike
Norwood, MA 02062

ABSTRACT

A phase Doppler particle analyzer (PDPA) was used to screen candidate water mist nozzles for use in a scaling validation aimed to allow scaled-down testing of water mist systems. Proper configuration of the PDPA remains somewhat of an art due to a lack of definitive guidelines for the many user-defined setup and data regression options. To validate the setup, a custom-designed iso-kinetic sampling probe (Probe) was developed to independently measure water mist fluxes at the same locations as the PDPA measurements. Using the Probe as a guide, the optimal PDPA operation parameters can be determined expeditiously for reliable measurements. To provide input to numerical modeling of water mist sprays, gross drop size distributions in terms of cumulative volume fraction were conventionally derived from local drop size distributions and water flux measurements and fitted using a composite of Rosin-Rammler and log-normal distributions. However, it was found that the accuracy of the data fit in the lower drop size range can substantially affect the conversion accuracy to the gross drop number distribution required by numerical modeling. This issue can be resolved by deriving the gross drop number distribution directly from measurements, or by ensuring a sufficiently accurate data fit in the lower drop size range if converted from the cumulative volume fraction.

KEYWORDS: phase doppler particle analyzer, iso-kinetic sampling, water mist sprays, scaling.

NOMENCLATURE LISTING

ΔA	local measurement area	R^V	local cumulative volume fraction
d	drop diameter	S	scaling ratio
GR^V	gross drop size distribution	t	test duration
GR^N	gross drop number distribution	$\dot{V}''$	water flux per unit area in the axial direction
L	length scale	**Subscripts**	
p	nozzle discharge pressure	*i*	location in spray cross-section
$\dot{Q}_w$	total water discharge rate	*j*	drop size bin
R^N	local cumulative number fraction		

INTRODUCTION

The phenomena governing water mist fire suppression are quite complex and not well understood quantitatively. Thus, the fire protection industry still relies primarily on the tried-and-true, but expensive, large-scale testing approach to develop water mist fire protection solutions. This makes the development of many potential applications economically prohibitive due to the high cost of constructing a full-scale testing mockup. The direct solution is a proven physical scaling protocol that allows the system development to be performed in a more affordable scaled-down facility. A series of fire suppression experiments conducted recently shows that a modification of a scale modeling originally developed thirty years ago is promising for use in scaling water mist fire suppression [1,2]. To ensure that appropriate water mist sprays were used in the scaling experiments, a 2-D phase Doppler particle analyzer (PDPA) was used to screen candidate nozzles.

The overall accuracy of the PDPA is strongly dependent on proper configuration of the system in terms of optics selection, laser beam intensity, alignment, signal amplification, and settings of drop signal acceptance criteria. The issue is particularly important for time-resolved data that rely not only on accurate measurement of each drop but also capture of each drop passing through the measurement area.

FIRE SAFETY SCIENCE–PROCEEDINGS OF THE NINTH INTERNATIONAL SYMPOSIUM, pp. 541-552
 / DOI:10.3801/IAFSS.FSS.9-541

For instance, a sufficiently large data sample is required to yield statistically meaningful drop size and velocity distributions. However, incorrectly applied signal acceptance criteria can cause improper acceptance or rejection of drop signals and detrimentally affect the overall measurement accuracy.

There are currently no standard procedures or known studies conducted to verify the accuracy of PDPA measurements for the types of sprays included in this study. An iso-kinetic sampling probe (Probe) was thus developed to independently measure water mist fluxes at the same locations as PDPA measurements for verification [3]. The configuration parameters of the PDPA can then be properly adjusted to ensure data quality.

The Froude-modeling-based scaling methodology calls for water mist sprays to follow prescribed scaling relationships for total water discharge rate, water discharge pressure, and drop size as shown in Table 1 below [1]. Table 2 shows the targeted water mist spray specifications used in the fire suppression experiments [2] based on the scaling requirements presented in Table 1. The two selected nozzles provide a scaling ratio of 3:1 and are correspondingly designated as the Scale-1 and Scale-3 nozzles.

This paper describes the water mist spray characterization of two selected nozzles with the following objectives: 1) detailed mapping of the spray characteristics to confirm the desired spray specifications can be obtained; 2) validation of PDPA mist flux measurements through independent mist flux measurements at specified locations in the spray; 3) use of mathematical functions to describe the gross drop size distribution of each spray for use in numerical simulations.

Table 1. Nozzle scaling parameters.

Length	$L_2/L_1=S$
Volumetric Water Discharge Rate	$\dot{Q}_{W,2} / \dot{Q}_{W,1} = S^{5/2}$
Drop Diameter	$d_2/d_1= S^{1/4}$
Discharge Pressure	$\Delta p_2 / \Delta p_1 =S$

Table 2. Targeted spray specifications.

Scale	Drop Size, d_{50}	Water Flow Rate	Discharge Pressure
-	(μm)	(l/min)	(kPa)
Scale-1	60	0.023	690
Scale-3	79	0.348	2068

MEASUREMENT APPARATUSES

Phase Doppler Particle Analyzer

Spray characterization experiments were conducted with a 2-component phase Doppler particle analyzer (PDPA) from TSI, Inc. The Phase Doppler Technique has existed for over 20 years and is accepted in the engineering and research community as an accurate and dependable method to measure fluid flow and particle characteristics. The PDPA uses light refracted from a water drop as the drop passes through the intersection of two monochromatic coherent laser beams to determine the trajectory and size of the drop [4]. The interference of the two coherent laser beams creates a fringe pattern (i.e. a series of light and dark lines) in a measuring volume that is defined by the ellipsoidal intersection area of the beams. The scattered light is collected by a receiver containing three detectors located off-axis from the laser beams. Each detector is located at a different elevation and therefore collects the same refracted light shifted slightly in phase. Differences in the phase shift are used to measure the drop characteristics. Each laser beam pair gives drop information relative to the orientation of the beams. Up to three pairs of laser beams, of different light wavelengths, can be used to acquire the three dimensions of drop movement [4].

The Gaussian nature of light intensity in the laser beams results in the necessity of several signal acceptance criteria to ensure validity and accuracy of drop measurements [4,5]. For instance, a very small

drop passing through the center, i.e. brightest portion, of the laser beam can scatter light with an intensity equivalent to a much larger drop passing through the outer edge of the beam. The result is a smaller effective measuring volume for small drops than for large drops. In addition, there are multiple setup options (laser beam intensity, off-axis angle of the receiver, alignment, slit aperture width, etc), which can affect the accuracy of drop measurements by optimizing signal strength. This is important because spray characteristics, such as drop density, can adversely affect the reliability of time-resolved data at a measurement location. For a water mist spray, the high drop density found at the spray centerline can result in a reduction in the signal-to-noise ratio causing erroneous drop rejection. Conversely, the relatively low drop density found near the edge can be insufficient to collect a large enough drop sampling size for statistical significance. Currently, there are no known definitive guidelines for the selection of signal acceptance criteria or the various setup options for the types of sprays typical in a water mist system [4,5].

In this investigation, a 300 mW air-cooled argon ion laser operating in multi-line mode was used as the illumination source. The laser beam transmitter and receiver were mounted on a rail assembly with rotary plates; a 40^{o} forward scatter collection angle was used. The transmitter had a focal length of 500 mm with an optical expander ratio of 2.0 and the receiver had a focal length of 500 mm. This resulted in a maximum measurable diameter size range of approximately 1 μm – 450 μm and ensured that the majority of drops were smaller than the beam waist at the measuring volume. Further information on operating conditions can be found in Reference [4,5].

Iso-Kinetic Sampling Probe

A custom-designed iso-kinetic sampling probe (Probe) was developed to independently measure water mist fluxes at the same locations where PDPA measurements were made [3]. This ensures proper operation of the PDPA system in terms of optics selection, laser beam intensity, alignment, signal amplification and settings of drop signal acceptance criteria.

Collecting the mist flux in the water mist spray is problematic because many of the drops are sufficiently small to follow the air currents of the spray. Therefore, a simple collection pan placed in the spray would not collect the drops in the spray that are small enough to follow air currents around and/or out of the pan. The Probe mitigates this problem by using a vacuum pump to generate a face velocity at the collection area equal to the air velocity in the water mist spray at that location. The internal structure of the Probe forces the coalescence of the drops preventing the drops from following the air currents through the tube and out through the vacuum pump. Water drops are collected in a reservoir tube, where the water level is measured with a differential pressure transducer. As shown in Fig. 1, a settling chamber is present in-line between the vacuum pump and the Probe to dampen pressure fluctuations.

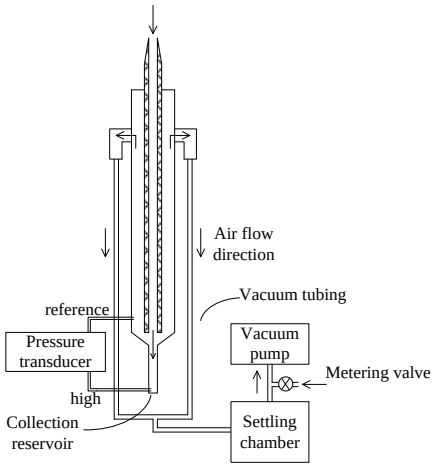

Fig. 1. Iso-kinetic sampling probe overview schematic (not to scale).

The face velocity of the Probe is measured with a hot wire anemometer without the presence of the water mist spray and adjusted with a metering valve located up-line from the vacuum pump. The Probe used for the Scale-1 nozzle had a circular collection area with a 2.66-cm diameter. The Probe was redesigned for the Scale-3 nozzle and had a circular collection area with a 1.8-cm diameter to increase measurement resolution. A PDPA test is run concurrent with each Probe test so the water flux measurements are directly comparable. Due to the large collection area of the Probe, relative to the PDPA measuring area, the PDPA water flux values are numerically integrated over the Probe measurement area to compare results. For each instrument, four measurements were obtained at each radial distance in the spray for averaging.

EXPERIMENTAL ARRANGEMENT

Spray Description and Experimental Setup

The water mist nozzles selected for testing had a full cone spray pattern with a $60^{o} \pm 10^{o}$ spray angle. A general schematic of the spray distribution can be seen in Fig. 2. The spray can be divided into two regimes; the momentum regime and the gravitation regime. The momentum regime occurs as water exits the nozzle and breaks up into small drops. In this portion of the spray the drops form a conical region. The center of the spray contains a higher concentration of smaller drops. The gravitation regime occurs after the drops begin to reach their respective settling velocities. The smaller drops are entrained into the spray core, which is formed by the air currents produced by the nozzle. The majority of spray water flux is contained in the spray core. The remainder of the larger drops has sufficient momentum to reach the outer edges of the spray.

With each nozzle discharging vertically downward, measurements were made for three discharge pressures. By mapping the nozzles at multiple pressures the spray characteristics of each nozzle can be correlated over a wide range of discharge pressures. At each discharge pressure, the local drop size distribution, water flux and mean drop velocity were mapped out across the horizontal cross-section of the spray at two elevations; one at the transition regime between the momentum-driven and the gravitational-driven regime of the spray and one in the gravitational regime of the spray, see Fig. 2. As shown in Fig. 3, each horizontal measurement plane was then divided into 24 equal areas using 25 measurement locations along two orthogonal diameters. Additional measurement locations near the center of the spray were added as necessary to provide higher resolution near the spray centerline. The edge of the spray was determined as the furthest radial distance from the spray centerline that drop data could be practically collected (i.e. minimum 100 drops in 5-min duration).

A Hago® 0.4-60B-DFN full cone nozzle was selected for Scale-1. The nozzle is rated to flow 0.023 l/min of water at 690 kPa. The three discharge pressures selected for testing were: 690, 1103, and 2068 kPa. The average diameter of the spray at the transition cross-section plane was 20 cm at 17 cm from the nozzle. The average diameter of the spray at the gravitational cross-section was 18 cm at 37 cm from the nozzle.

A Spraying Systems® LN02 nozzle was selected for Scale-3. The nozzle is rated to flow 0.348 l/min of water at 2068 kPa. The three discharge pressures selected for testing were: 1034, 2068, and 4127 kPa. The average diameter of the spray at the transition cross-section was 56 cm at 40 cm from the nozzle. The average diameter of the spray at the gravitation cross-section was 52 cm at 62 cm from the nozzle.

The nozzles were mounted on a 3-D traverse allowing motion in a space measured approximately 3.1 m x 3.1 m x 3.6 m high, while the PDPA's measuring volume remained stationary. The nozzle was secured in place on a 25.4-cm square platform. The piping on the nozzle platform consisted of stainless-steel pipe and fittings secured to an aluminum plate with rubber gasket pipe brackets. Nozzle pressure was measured with a 0-2068 kPa pressure gauge for low pressure tests and a 0-10,342 kPa pressure gauge for high pressure tests.

Water flow to the nozzle was accomplished by pressurizing a water storage tank with dry grade nitrogen. The nitrogen supply pressure was regulated with a two stage regulator and the tank pressure was monitored with a pressure gauge. The water tank was connected to the nozzle platform with a high pressure flexible tube.

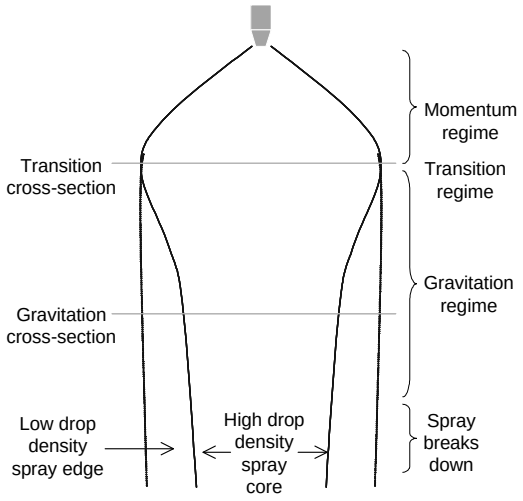

Fig. 2. Spray measurement elevations.

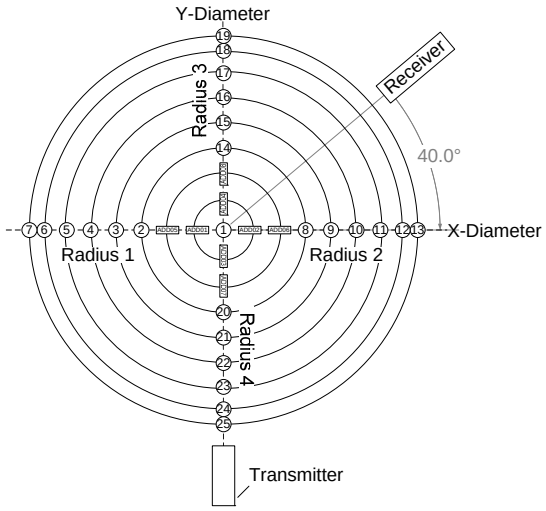

Fig. 3. Measurement locations for each horizontal cross-section (not to scale).

PDPA RESULTS AND DISCUSSION

A total of 12 measurement series were conducted with the PDPA, including two cross-sections and three discharge pressures for each nozzle. The Probe was used to establish the PDPA configuration for each nozzle and was not used in all series. For simplicity, only data for each nozzle at the target discharge pressure are presented, i.e. 690 kPa for Scale-1 and 2068 kPa for Scale-3. The data presented in this paper is temporal, which refers to measurements made with respect to time. Temporal data can be converted to spatial data, which refers to measurements made with respect to unit volume, by dividing by the drop velocity and vice versa.

For illustration, a series of graphs for drop diameter, mist flux, and mean drop velocity as a function of normalized radius are given in Fig. 4 through 7 for the Scale-1 and Scale-3 nozzles. For each graph, positive radius location represents the average of the corresponding locations in Radii 1 and 2 of the X-diameter. Similarly, negative radius location represents the average of the corresponding locations in Radii 3 and 4 of the Y-diameter.

As shown in Fig. 4, the volume median diameter profile for each nozzle resembles an inverse bell-curve distribution. Figures 5 and 6 show the mist flux profile of the Scale-1 and Scale-3 nozzles to have an approximate bell-curve distribution, with the farthest three measurements from the centerline contributing little to the overall flow of the spray. The reduced mist flux near the spray centerline of the Scale-3 nozzle can be primarily attributed to the high concentration of smaller drops.

It is convenient to represent the drop velocity profile of a spray with the vertical mean velocity of the volume-median-diameter drop for each measurement location. This excludes any lateral spray motion. Figure 7 shows the mean vertical velocity of the volume-median-diameter drop as a function of normalized radial distance at the gravitation cross-section in the spray for each nozzle. In all cases, the drop velocity profile resembles a bell-curve distribution.

Figures 8 and 9 show the radial velocity of the spray for the Scale-1 and Scale-3 nozzles, respectively, along the X-diameter for their target pressure at the transition cross-section. The mean radial velocity at each location is plotted versus radial distance normalized by the spray radius. However, plotting mean lateral drop velocity alone can be misleading as lateral motion for different drops can occur in opposing directions. Therefore, each plot includes ± one standard deviation of the velocity to show the variation at each measurement location. Positive velocities represent motion toward the spray edge and negative velocities represent motion toward the spray center.

For both nozzles, the radial drop motion exhibits a large amount of variation near the spray center and the spray edges with a slight mean inward velocity at both locations. These are expected trends. The variation

of drop motion near the spray center and slight inward drop motion result from entrainment of drops into the air currents produced by the nozzle. Variation of drop motion at the spray edge results from a low drop density exaggerating the importance of each drop measurement and the inward motion of drops results from the minor negative pressure at the spray core caused by air current produced by the nozzle. Though not shown, the degree of variation in the radial velocity in the spray core at the gravitation cross-section is comparable to that at the transition cross-section, while the variation at the spray edge is reduced significantly.

More insight into the development of the spray can be gained by looking at the local cumulative volume fraction (CVF) for each measurement location in the spray. The local CVF is the cumulative percentage of all drops below a given size divided by the total volume of drops collected at that location. The CVF for each measurement location along the X-diameter axis is given in Fig. 10 and 11 for the Scale-1 and Scale-3 nozzles, respectively. These data highlight the symmetry and development of the spray with respect to the drop size distribution as a function of radial distance from the vertical centerline. As expected with a full cone nozzle, the diameter of the drops increases with radial distance from the spray centerline.

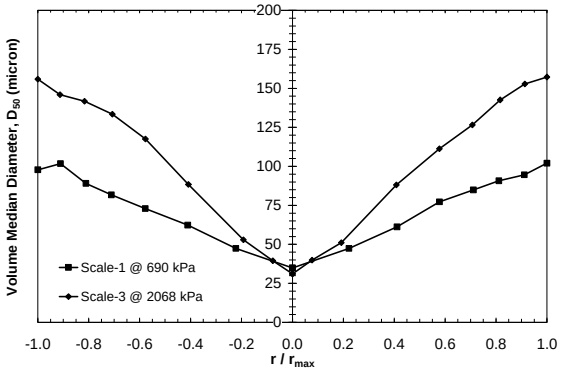

Fig. 4. Average drop diameter profile for Scale-1 and Scale-3 nozzles at the gravitation cross-section.

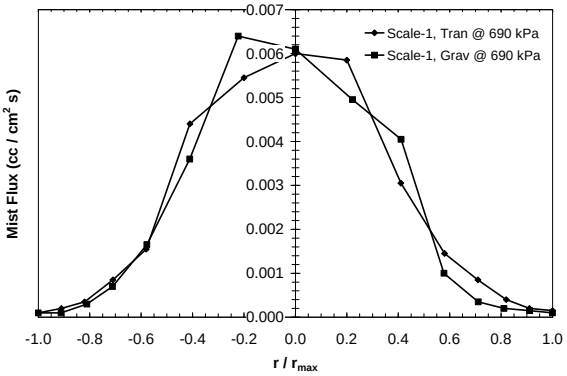

Fig. 5. Mist flux profile for Scale-1 nozzle at the gravitation cross-section.

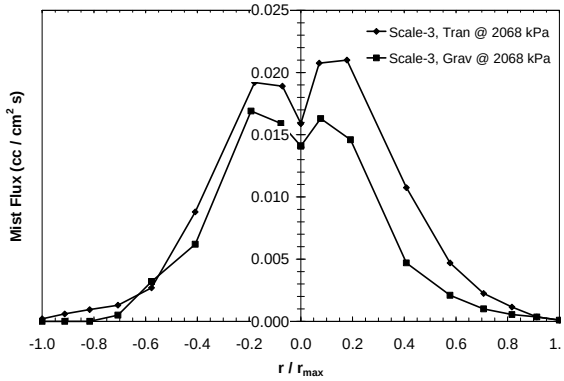

Fig. 6. Mist flux profile for Scale-3 nozzle at the gravitation cross-section.

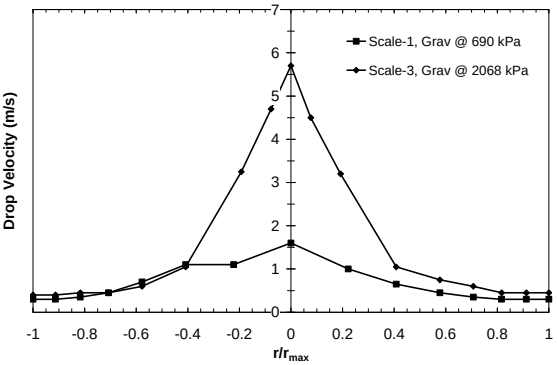

Fig. 7. Mean velocity profile of the volume median diameter for Scale-1 and Scale-3 nozzles at the gravitation cross-section.

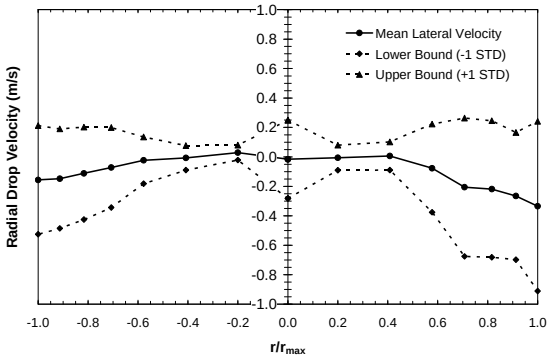

Fig. 8. Radial velocity profile for Scale-1 nozzle with a 690 kPa discharge pressure at the transition cross-section.

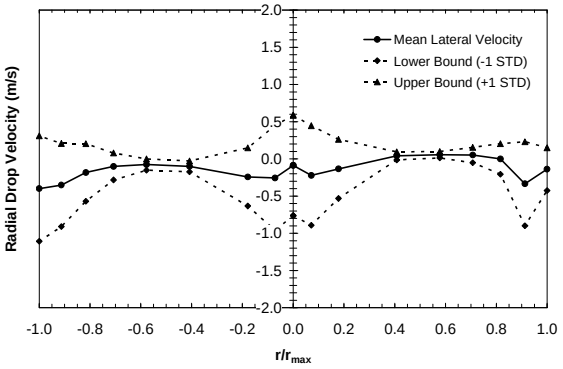

Fig. 9. Radial velocity profile for Scale-3 nozzle with a 2068 kPa discharge pressure at the transition cross-section.

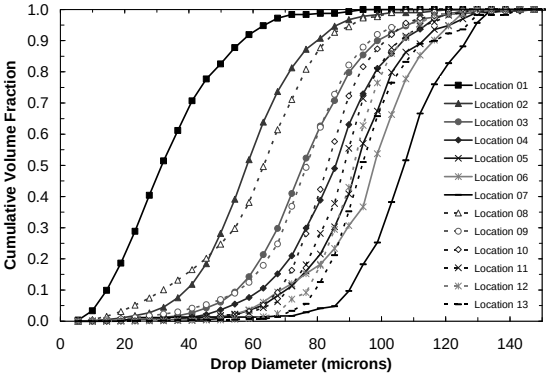

Fig. 10. Scale-1 cumulative volume fraction in the gravitation cross-section at 690 kPa.

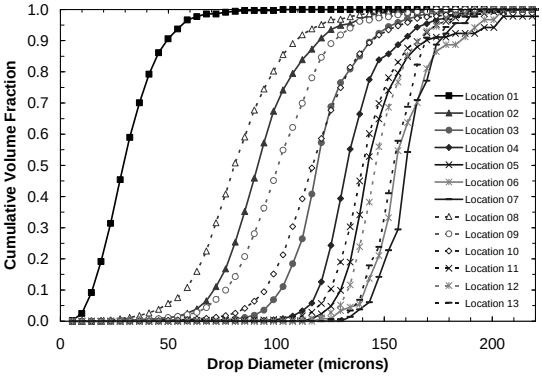

Fig. 11. Scale-3 cumulative volume fraction in the gravitational regime at 2068 kPa.

PROBE RESULTS AND DISCUSSION

Mist flux measurements were also taken with the Probe for each nozzle at the gravitation cross-section. Water flux data obtained with the PDPA are numerically integrated over the Probe collection area so that a comparison can be made between the two values over the same measurement area. The comparison does not include the outer two measurement locations. The drop number concentration at the spray edge is substantially lower than that at the spray core, which significantly increases the impact of each PDPA drop detection and reduces the measurement reliability. The low mist flux present near the spray edge also makes the time to collect an adequate amount of water with the Probe prohibitively long.

For the Scale-1 nozzle, the discharge pressure was set to 690 kPa providing a water discharge rate of 0.023 l/min. In general, there was good agreement between the mist fluxes measured from the PDPA and Probe when the PDPA operated with optimal operating parameters. As seen in Fig. 12, the difference between the fluxes increases towards the spray core where the Probe measures a higher flux than the PDPA. The overall agreement between PDPA and Probe measured mist fluxes was within 20% for the high drop density spray core, with the exception of the centerline measurement which was 30%. This may be attributed to an insufficient number of data points and the higher rejection rate of PDPA drop signals in the high density core region of the spray, which extends to approximately 5 cm from the spray centerline at an elevation of 37 cm below the nozzle, to resolve the actual distribution.

For the Scale-3 nozzle, two changes were made to increase the mist flux comparison reliability; 1) an additional measurement location was added near the spray centerline, and 2) the Probe was redesigned to have a reduced collection area, of approximately 1.8-cm diameter reduced from 2.54-cm diameter. Figure

13 shows the comparison of PDPA data and Probe data for the Scale-3 nozzle with a discharge pressure of 2068 kPa, providing a water discharge rate of 0.348 l/min. The overall agreement between PDPA and Probe measured mist fluxes was within 10% for the high drop density spray core, again with the Probe measuring slightly higher mist fluxes in the spray core. For this nozzle, the spray core extended to approximately 10 cm from the spray centerline at an elevation of 52 cm below the nozzle.

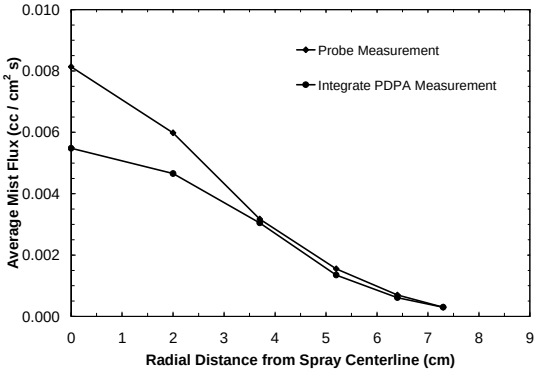

Fig. 12. Scale-1 comparison of mist flux measurements in the gravitation cross-section at 690 kPa.

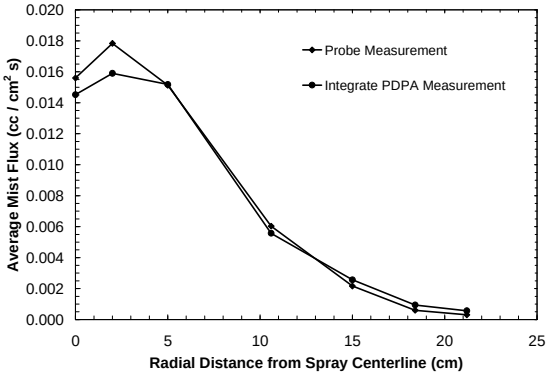

Fig. 13. Scale-3 comparison of mist flux measurements in the gravitation cross-section at 2608 kPa.

CONSERVATION OF WATER FLOW

The actual flow rate from the nozzle was measured by collecting the water flow through each nozzle at all three discharge pressures for one minute. In all cases, the collected flow rate was within 10% of the manufacturer's specification. Table 3 contains a list of the actual flow rates for both nozzles at each discharge pressure based on manufacturer specifications.

Two methods were considered for calculating the total flow rate from the experimental data. In both cases, mist flux data from the PDPA was first plotted versus radial distance from the spray centerline. The resulting plots were then; 1) fitted with a best-fit polynomial curve and integrated with respect to radial distance, and 2) numerically integrated with respect to radial distance without the curve fit.

Fitting the data with a polynomial best-fit curve proved to be an ineffective method of accurately representing mist flux plots. For the limited number of measurements taken for each spray radius, no greater than a 3rd order polynomial should be considered due to increased uncertainty inherent to higher order polynomials. Unfortunately, it was found that at least a 5th order polynomial was necessary to provide an acceptable fit to the data distribution pattern. The resulting total flow calculations varied by up to 40% depending on the order of the polynomial used (i.e. 5th, 6th, or 7th order), while the curves fit the data almost identically with R^2 values greater than 0.998. The magnitude of the variance was unacceptable and the results are therefore not reported.

Total flow calculations using the second integration method following the trapezoidal rule are compared against actual flow rates in Table 3. The second integration method was advantageous over the first integration method as there are no issues with reliability of the data fit. For the discharge pressures included in this paper, the calculated total flows were within 21% of the actual flow for the Scale-1 nozzle and 25% of the actual flow for the Scale-3 nozzle. Errors in the calculated flow rate are expected due to the strong dependence on accurate measurement of the local mist flux. Any variance in the measured drop size and velocity with the PDPA are then compounded for the mist flux calculation, particularly for the outer periphery of the spray where the low drop density reduces the drop sampling size and the core of the spray where the high drop density can cause a higher rejection rate of PDPA drop signals.

Table 3. Total flow rate comparison for all three scales at the gravitation cross-section.

Scale	Pressure (kPa)	Actual Flow Rate (l/min)	Calculated Flow Rate (l/min)	Difference (%)
1	690	0.023	0.023	0
	1103	0.028	0.022	21
	2068	0.039	0.040	3
3	1034	0.246	0.287	17
	2068	0.348	0.371	7
	4137	0.492	0.564	25

A convenient method of comparing spray patterns between nozzles is the radial distribution of water flux compared to the mean water flux in a spray cross-section. Figure 14 shows the mist flux distributions for each nozzle normalized by the mean mist flux value over the entire cross-section as a function of the radial distance normalized by the spray radius. This allows comparison of spray patterns irrespective of spray diameters or overall water discharge rates. The Scale-1 and Scale-3 nozzles show good agreement at both the transition and gravitation cross-sections. This is consistent with the trend found in the drop size distribution and non-normalized mist flux distribution with respect to radial distance. At the transition cross-section, the mean mist flux for the Scale-1 and Scale-3 are 0.274 cc/cm^2*s and 0.3041 cc/cm^2*s, respectively. At the gravitation cross-section, the mean mist flux for the Scale-1 and Scale-3 nozzles are 0.254 cc/cm^2*s and 0.287 cc/cm^2*s, respectively.

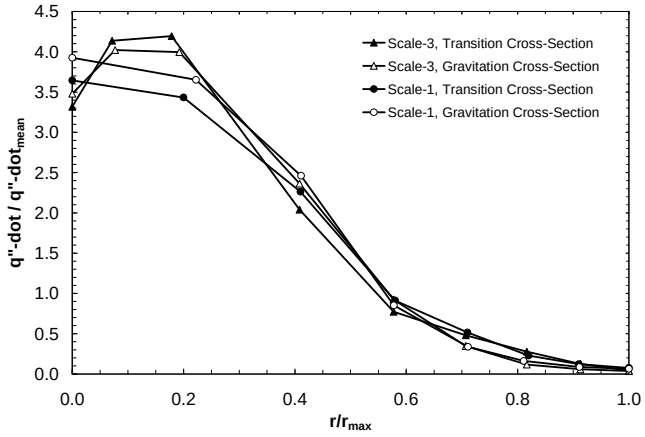

Fig. 14. Normalized mist flux as a function of normalized radial distance for the Scale-1 and Scale-3 nozzles.

GROSS DROP SIZE DISTRIBUTION FOR NUMERICAL MODELING

Many studies have been conducted to quantify the fire suppression mechanisms of water mist systems [6,7], which require a mathematical representation of the spray characteristics. Using PDPA data, the gross CVF distribution was derived from the local measurements by integrating the measurements in the entire spray cross-section [8,9]. The local CVF measurements are weighted by the corresponding mist flux and measurement area with the equation below:

$$GR_j^V = \frac{\sum R_{i,j}^V \text{ x } \Delta A_i \text{ x } \dot{V}''}{\sum \Delta A_i \text{ x } \dot{V}''}, \qquad (1)$$

where $R_{i,j}^{V}$ is the cumulative volume fraction for all drop sizes equal to and less than d_j at location *i*, ΔA_i is the local area centered at Location *i*, and $\dot{V}''$ is the local mist flux.

The volume median diameter was taken as the 50% point of the gross CVF distribution. Figure 15 shows a comparison of the gross drop size distribution for both nozzles at the targeted pressures. In both cases the median drop sizes were within 10% of the target values. As the water flow rate increases from Scale-1 to Scale-3, the total range of drop sizes present in the spray also increases. To make comparison on the same basis, Fig. 16 shows the gross drop size distributions for both nozzles normalized by the respective volume median diameters. The agreement of the two data sets shows that overall each nozzle generates a spray consisting of a similar distribution pattern.

For numerical modeling of a spray, it is convenient to provide a mathematical representation of the gross CVF distribution. Conventionally for water sprays a composite of two distributions is used to describe the gross CVF distribution: a log-normal distribution for the small drops and a Rosin-Rammler distribution for the large drops [8,10]. Figures 17 and 18 show two different data fits for the Scale-1 nozzle at its target pressure in the gravitation cross-section, labeled data fit #1 and #2, respectively. For data fit #1, a log-normal distribution was used to represent the smallest drop diameters, resulting in a fit for drop sizes less than or equal to $d / d_m = 0.67$. A more typical approach was taken in data fit # 2 with a log-normal distribution fitting drop diameters less than $d / d_m = 1$. In both cases a Rosin-Rammler distribution was used to fit the remaining drops. Both data fits agree well for the upper portion of the drop distribution, while the lower portion of the drop distribution was better represented in data fit #1.

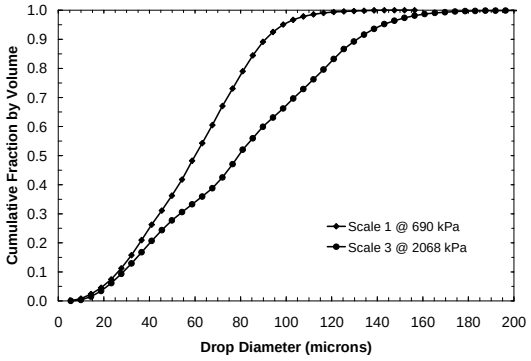

Fig. 15. Comparison of gross CVF distributions of Scale-1 and Scale-3 nozzles in the transition cross-section.

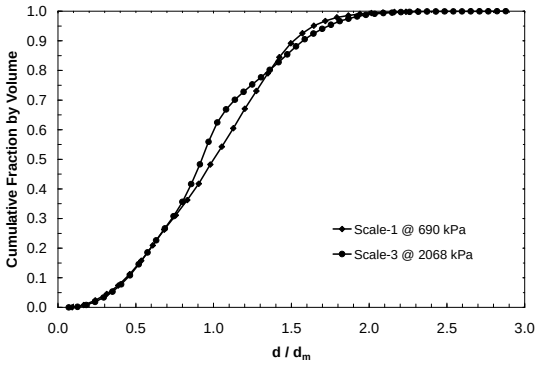

Fig. 16. Comparison of normalized gross CVF distributions of Scale-1 and Scale-3 nozzles in the transition cross-section.

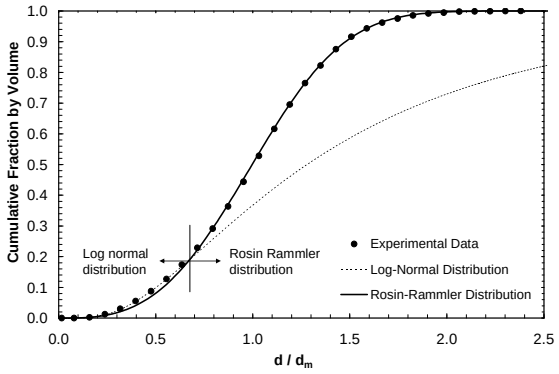

Fig. 17. Composite data fit # 1 for Scale-1 gross CVF distribution in the gravitation cross-section at 690 kPa.

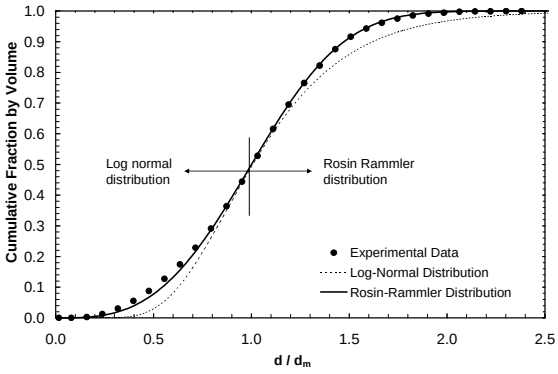

Fig. 18. Composite data fit # 2 for Scale-1 gross CVF distribution in the gravitation cross-section at 690 kPa.

Another way of representing a spray for modeling purposes is the gross drop number distribution. This supports the actual spray information requirement for numerical simulation of water sprays, Fire Dynamics Simulator for example [11], e.g. specific number of drops for each representative drop diameter. The experimentally determined gross drop number distribution is calculated in a manner similar to the gross CVF distribution. Individual drop measurements for each location in the spray are used to generate the local cumulative number fraction (CNF), which represents the cumulative number of drops below a given drop size divided by the total number of drops at that location. The gross CNF distribution can then be derived from the corresponding local measurements by performing area integration. The measurement locations are weighted by the measurement area and total number of drops as follows:

$$GR_j^N = \frac{\sum \left(N_i / t_i\right) \times R_{i,j}^N \times \Delta A_i}{\sum \Delta A_i \left(N_i / t_i\right)} \qquad (2)$$

where N_i is the number of drops measured at Location *i*, t_i is measurement time at Location *i*, $R_{i,j}^N$ is the cumulative number fraction for drop sizes equal to and less than d_j at Location *i*, and ΔA_i is the local area centered at Location *i* at which N_i is measured.

In principle the gross CNF distribution can be derived from the gross CVF distribution by dividing by the cube of the diameter and integrating the result. However, the accuracy of the resulting distribution is strongly dependent on the quality of the data fit, particularly in the lower drop size range. To highlight this, the two data fits of the gross CVF distribution presented in Fig. 17 and 18 are converted to the corresponding gross CNF distribution and compared to the experimentally calculated gross CNF distribution in Fig. 19. By using the log-normal distribution to accurately represent the lower drop size range and Rosin-Rammler distribution to represent the remainder of the drop size range, the gross CNF distribution derived from data fit #1 agrees well with the experimental gross CNF distribution. Conversely, using the conventional method of fitting drops smaller than d_m with a log-normal distribution and drops larger than d_m with a Rosin-Rammler distribution, the gross CFN distribution derived from data fit #2 underestimates the lower drop diameter range of the gross CVF distribution and consequently provides poor agreement with the experimental gross CNF distribution. To further highlight the sensitivity to the data fit in the lower drop diameter range, the gross CNF distribution was also calculated using the Rosin-Rammler distribution included in data fit #1 to represent the entire drop range. Compared to the composite data fit only a minor underestimation of the lower drop diameter range of the gross CVF distribution exists, however the resulting gross CNF distribution shows considerable error.

The data obtained in this study can be used to fine-tune and validate numerical spray transport models. The validated models can then be used to calculate sprays under other nozzle operating conditions.

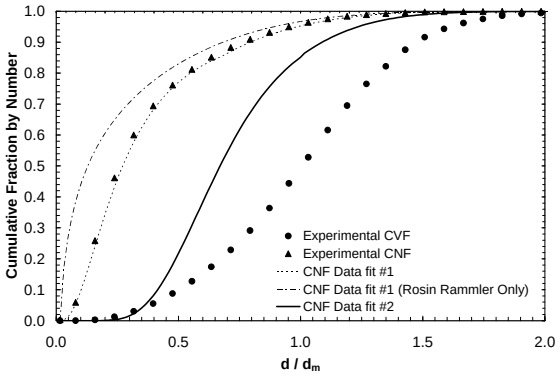

Fig. 19: Comparison of gross CNF distribution data fits for Scale-1 nozzle in the gravitation cross-section at 690 kPa

SUMMARY AND CONCLUSIONS

The water mist sprays of two single-fluid nozzles have been characterized using a 2-D PDPA and an iso-kinetic sampling probe. The latter has proven to be useful in achieving optimal PDPA operating conditions and configuring post-processing routines to produce reliable measurements. It was found that the accuracy of the data fit of the gross cumulative volume fraction distribution in the lower drop size range can greatly affect the conversion accuracy to the equivalent cumulative number fraction distribution. This issue can be resolved by deriving the gross drop number distribution directly from measurements, or by ensuring a sufficiently accurate data fit in the lower drop size range if converted from the cumulative volume fraction. Accurate representation of the starting gross drop number distribution of a spray is essential for reliable predictions of numerical spray transport models.

ACKNOWLEDGMENTS

The authors would like to thank Danny Zielinski for the design and construction of the nozzle traverse apparatus and Drs. Jukka Varri of VTT and Xiangyang Zhou of FM Global for helpful discussions on numerical simulations.

REFERENCES

[1] Yu, H-Z, "Froude-Modeling-Based General Scaling Relationships for Water-Spray-Fire-Plume Interactions," Fire Safety Science – Proceedings of 7th Asia-Oceania Symposium on Fire Science and Technology, International Association of Fire Safety Science, 2007.

[2] Jayaweera, T.M. and Yu, H-Z, (in press) "Scaling of Fire Cooling by Water Mist Under Low Drop Reynolds Number Condition," Fire Safety Journal, don:10.1016/j.firesaf.2007, 01.004.

[3] Ditch, B., Yu, H-Z, "Characterization of Mist Sprays Using a Phase-Doppler Particle Analyzer and an Iso-kinetic Sampling Probe," US Patent 7,181,952, February 27, 2007.

[4] Albrecht, H.E., Borys, M., Damaschke, N., Tropea, C., *Laser Doppler and Phase Doppler Measurement Techniques*, Springer-Verlag Berlin Heidelberg, Germany, 2003.

[5] TSI Inc., "Phase Doppler Particle Analyzer (PDPA) and Laser Doppler Velocimeter (LDV) Operations Manual," St. Paul, MN USA, December, 2001.

[6] Hostikka, S., McGrattan, K, "Numerical modeling of radiative heat transfer in water sprays," Fire Safety Journal, Journal 41 (2006), p. 76-86

[7] Yoona, S., Kima, H., and Hewsonb, J., "Effect of initial conditions of modeled PDFs on droplet characteristics for coalescing and evaporating turbulent water spray used in fire suppression applications," Fire Safety Journal, Volume 42 (2007), doi:10.1016/j.firesaf.2007.01.001

[8] Yu, H.-Z., "Investigation of Spray Patterns of Selected Sprinklers with the FMRC Drop Size Measuring System," *Proceedings of the First International Symposium on Fire Safety Science*, Hemisphere Publishing Corporation, 1986.

[9] "NFPA 750 - Standard on Water Mist Fire Protection Systems, 2003 Edition," National Fire Protection Association, 2003

[10] Lefebvre, A.H., *Atomization and Sprays*, Hemisphere Publishing Corporation, USA, 1989

[11] McGratten, K., Forney, G., Fire Dynamics Simulator (Version 4) User's Guide, NIST Special Publication 1019, March, 2006.